Chaos, Solitons and Fractals 139 (2020) 110300

Contents lists available at ScienceDirect

Chaos, Solitons and Fractals

Nonlinear Science, and Nonequilibrium and Complex Phenomena

journal homepage: www.elsevier.com/locate/chaos

Periodic travelling wave solutions for a reaction-diffusion system on landscape fitted domains

Sangkwon Kim[a], Jintae Park[a], Chaeyoung Lee[a], Darae Jeong[b], Yongho Choi[c], Soobin Kwak[a], Junseok Kim[a,*]

[a] Department of Mathematics, Korea University, Seoul 02841, Republic of Korea
[b] Department of Mathematics, Kangwon National University, Gangwon-do 24341, Republic of Korea
[c] Department of Mathematics and Big Data, Daegu University, Gyeongsan-si, Gyeongsangbuk-do 38453, Republic of Korea

ARTICLE INFO

Article history:
Received 12 June 2020
Revised 3 August 2020
Accepted 13 September 2020
Available online 21 September 2020

Keywords:
Distance function
Periodic travelling waves
Reaction-diffusion system
Landscape features

ABSTRACT

In this article, we propose a new landscape fitted domain construction and its boundary treatment of periodic travelling wave solutions for a diffusive predator-prey system with landscape features. The proposed method uses the distance function based on an obstacle. The landscape fitted domain is defined as a region whose distance from the obstacle is positive and less than a pre-defined distance. At the exterior boundary of the domain, we use the zero-Neumann boundary condition and define the boundary value from the bilinearly interpolated value in the normal direction of the distance function. At the interior boundary, we use the homogeneous Dirichlet boundary condition. Typically, reaction-diffusion systems are numerically solved on rectangular domains. However, in the case of periodic travelling wave solutions, the boundary treatment is critical because it may result in unexpected chaotic pattern. To avoid this unwanted chaotic behavior, we need to use sufficiently large computational domain to minimize the boundary treatment effect. Using the proposed method, we can get accurate results even though we use relatively small domain sizes.

1. Introduction

Many mathematical models for spatial dynamics of predator-prey populations have considered that populations are distributed in uniform environments. However, landscape features can significantly inhibit the migration of the populations [1]. The authors in Sherratt et al. [2] studied the effects of the size and shape of landscape features on the standard predator-prey dynamics using periodic travelling waves. They showed that the size rather than the shape of an obstacle determines the property of wave-forming. Babloyantz and Sepulchre [3] studied wave propagation in oscillatory media with obstacles. They showed that waves can only propagate to windows if the windows' width exceeds the critical width, and waves that propagate to two neighboring windows of different width can affect each other. In [4], the authors performed systematic studies on how obstacle size affects the wavelength and amplitude of the selected waves. They derived a leading order approximation to the wave generated by the landscape feature, using perturbation theory. As a result, the authors showed that on a flat boundary, the limit values of amplitude and wavelength are not exponentially approaching, however rather algebraically approaching with distance from the edge of an obstacle. In [5], the authors studied the travelling wave solution for a reaction-diffusion system. For the regular periodic travelling wave solutions in spatio-temporal oscillations, a numerical algorithm was proposed to detect one-period of travelling wave solutions. Garvie et al. [6] studied with spatially extended predator-prey dynamics using the finite element method (FEM) on two-dimensional arbitrarily shaped domains and presented ecologically relevant experiments to investigate the effects of habitat shapes, boundary conditions, and initial conditions determining the spatio-temporal dynamics. In [7], a reaction-diffusion model was investigated for the condition which has a unique positive constant solution, the property of the equation for the large time behaviors of the nonconstant solutions, and asymptotic stability of the positive constant solution. In [8], reaction-diffusion equations were chosen to mathematically describe the spread of alien species. Here, the authors noted the study of patterns and proportions of invasive species in complex domains rather than in open domains. Specifically, an H-shaped domain with two rectangular habitats connected by a narrow passage was considered. Through numerical simulations with various initial conditions and parameters, it

* Corresponding author.
E-mail address: cfdkim@korea.ac.kr (J. Kim).
URL: http://math.korea.ac.kr/~cfdkim/ (J. Kim)

https://doi.org/10.1016/j.chaos.2020.110300
0960-0779/

was found that the complex domain produced important pattern results of spreading species. Yue et al. [9] considered a new irregular domain, using a new space-time radial basis function method, for a nonhomogenous convection-diffusion model. The authors introduced the new space-time method from distance perspective on objects and presented the numerical results showing its efficiency in solving long-time and large-scale problems. Sherratt [10] studied the numerical continuation methods for the periodic travelling waves. Sherratt described the calculation of boundaries in parameter space for the existence and stability of periodic travelling waves in the Klausmeier model for banded vegetation in semi-arid environments. In [11,12], the authors studied a reaction-diffusion model of cardiac excitation that exhibits spiral wave instability in the two-dimensional spatial domains. To describe the spiral wave instability, they presented numerically the existence of periodic travelling wave solution and the emergence of a stable spiral pattern before the bifurcation point. A recent discovery of the vegetation in the form of a spiral in arid dryland is drawing attention. Interpretation of phenomena appearing in the vegetation spiral and numerical modeling regarding the observation was studied [13]. However, the vegetation spiral is not only not a wave, but it also does not rotate. According to Bordeu et al. [14], the curvature instability which affects the circular-shaped vegetation patch leads to the elliptical-shaped of the vegetation patch. Recently, Smith et al. [15] investigated the damage and recovery of two-dimensional reaction-diffusion wavefronts with obstacles. By solving the Tyson–Fife model with the finite difference method (FDM), they presented the numerical simulation results with various obstacles and their conditions (shape, size, aspect ratio, and orientation). They found that the recovery of the wave could be utilized to explain the effect of imbalance on the recovery of the wavefront in cardiac tissue.

Commonly, chaotic dynamics can occur with some range of model parameter values [16–19]. However, when predator-prey systems are numerically solved on rectangular domains, especially in the case of periodic travelling wave solutions, the appropriate boundary treatment is critical because it may result in unexpected chaotic patterns that are not from the governing equations but from the numerical errors. To resolve the reflective boundary problems, in this paper, we propose a novel numerical method for periodic travelling wave solutions for predator-prey systems on arbitrarily shaped landscape domains. In the proposed method, we define a distance function based on an obstacle. Using the distance function, the landscape fitted computational domain is defined as a region whose distance from the obstacle is positive and less than a pre-defined distance. At the exterior boundary of the domain, we use the zero-Neumann boundary condition and define the boundary value from the bilinearly interpolated value in the normal direction of the distance function.

The rest of the paper is structured as follows. In Section 2, the predator-prey system is presented. In Section 3, the proposed numerical method is described in detail. In Section 4, several computational results are presented. Conclusions are given in Section 5.

2. The governing system

In this article, we consider the following reaction-diffusion equations [1]:

$$\frac{\partial u}{\partial t}(\mathbf{x},t) = D_u \Delta u(\mathbf{x},t) + \frac{aku(\mathbf{x},t)v(\mathbf{x},t)}{1+kv(\mathbf{x},t)} - bu(\mathbf{x},t),\ \mathbf{x}\in\Omega,\ t>0, \tag{1}$$

$$\frac{\partial v}{\partial t}(\mathbf{x},t) = D_v \Delta v(\mathbf{x},t) + rv(\mathbf{x},t)\left(1-\frac{v(\mathbf{x},t)}{v_0}\right) - \frac{cku(\mathbf{x},t)v(\mathbf{x},t)}{1+kv(\mathbf{x},t)}, \tag{2}$$

where $\Omega \subset \mathbb{R}^2$ is a domain, u and v are predator and prey populations, respectively. This model is based on the field vole (prey)–weasel (predator) interaction. Let us define the non-dimensional parameters as $u^* = uc/(rh_0)$, $v^* = v/v_0$, $t^* = rt$, $\mathbf{x}^* = \sqrt{r/D_v}\mathbf{x}$, $\delta^* = D_u/D_v$, $A^* = a/b$, $B^* = r/a$, $C^* = kv_0$. Then, Eqs. (1) and (2) become the following non-dimensional equations after dropping the asterisks:

$$\frac{\partial u}{\partial t}(\mathbf{x},t) = \delta \Delta u(\mathbf{x},t) + \frac{u(\mathbf{x},t)}{AB}\left(\frac{ACv(\mathbf{x},t)}{1+Cv(\mathbf{x},t)} - 1\right), \tag{3}$$

$$\frac{\partial v}{\partial t}(\mathbf{x},t) = \Delta v(\mathbf{x},t) + v(\mathbf{x},t)(1-v(\mathbf{x},t)) - \frac{Cu(\mathbf{x},t)v(\mathbf{x},t)}{1+Cv(\mathbf{x},t)}. \tag{4}$$

3. Numerical method

We define a rectangular domain $\Omega = (L_x, R_x)\times(L_y, R_y)$ embedding an obstacle region, Ω_o, see Fig. 1(a). Let us discretize the two-dimensional domain Ω using a uniform spatial step size $h = (R_x - L_x)/N_x = (R_y - L_y)/N_y$, where N_x and N_y are positive integers. Let $\Omega^h = \{(x_i, y_j) | x_i = L_x + (i-1)h,\ 1 \le i \le N_x$ and $y_j = L_y + (j-1)h,\ 1 \le j \le N_y\}$ be a discrete domain and Ω_o^h be the discrete obstacle domain. The numerical solutions to $u(x, y, t)$ and $v(x, y, t)$ are approximated at cell-corners by $u_{ij}^n \equiv u(x_i, y_j, n\Delta t)$ and $v_{ij}^n \equiv v(x_i, y_j, n\Delta t)$, where Δt is the temporal step size. We define the unsigned discrete distance function ϕ_{ij} on Ω^h from Ω_o^h (see Fig. 1(c)), i.e.,

$$\phi_{ij} = \min_{(x_p,\ y_q)\in\Omega_o^h} \sqrt{(x_i - x_p)^2 + (y_j - y_q)^2},\ 1 \le i \le N_x \text{ and } 1 \le j \le N_y.$$

Then, we define the discrete computational domain Ω_c^h (see Fig. 1(d)) as

$$\Omega_c^h = \bigcup_{0<\phi_{ij}<d} \{(x_i, y_j)\},\quad \text{for some}\ \ d > 0. \tag{5}$$

We solve the following discrete Eqs. (6) and (7) on Ω_c^h:

$$\frac{u_{ij}^{n+1} - u_{ij}^n}{\Delta t} = \delta \Delta_d u_{ij}^n + \frac{u_{ij}^n}{AB}\left(\frac{ACv_{ij}^n}{1+Cv_{ij}^n} - 1\right), \tag{6}$$

$$\frac{v_{ij}^{n+1} - v_{ij}^n}{\Delta t} = \Delta_d v_{ij}^n + v_{ij}^n\left(1 - v_{ij}^n\right) - \frac{Cu_{ij}^n v_{ij}^n}{1+Cv_{ij}^n}, \tag{7}$$

where the discrete Laplacian is defined as $\Delta_d u_{ij}^n = (u_{i+1,j}^n + u_{i-1,j}^n + u_{i,j+1}^n + u_{i,j-1}^n - 4u_{ij}^n)/h^2$. The computational domain boundary $\partial\Omega_c^h$ consists of two types of boundaries: obstacle boundary $\partial\Omega_o^h$ and exterior boundary $\partial\Omega_e^h$, i.e., $\partial\Omega_c^h = \partial\Omega_o^h \cup \partial\Omega_e^h$. At the obstacle boundary, we set the zero Dirichlet boundary condition as $u_{ij}^n = v_{ij}^n = 0$ for $(x_i, y_j) \in \partial\Omega_o^h$. On the exterior boundary $(x_i, y_j) \in \partial\Omega_e^h$, we compute the inward unit normal vector

$$\mathbf{n} = -\frac{\nabla_d \phi_{ij}}{|\nabla_d \phi_{ij}|}, \tag{8}$$

where $\nabla_d \phi_{ij} = \left((\phi_x)_{ij},\ (\phi_y)_{ij}\right) = \left(\frac{\phi_{i+1,j} - \phi_{i-1,j}}{2h},\ \frac{\phi_{i,j+1} - \phi_{i,j-1}}{2h}\right)$.

We define $u_{ij}^n = u^n((x_i, y_j) + H\mathbf{n})$, where H is an interpolation length and should be greater than $\sqrt{2}h$ to make sure that $(x_i, y_j) + H\mathbf{n}$ is surrounded by four interior points of a unit cell in Ω_c^h. To define the value of $u^n((x_i, y_j) + H\mathbf{n})$, we use the bilinear interpolation from the values at the four points of the unit cell. Using the same procedure, we compute $v_{ij}^n = v^n((x_i, y_j) + H\mathbf{n})$ at the exterior boundary $(x_i, y_j) \in \partial\Omega_e^h$, see Fig. 1(e). In previous studies [1,2,4], the boundary conditions are chosen as zero densities (Dirichlet boundary condition) at the edge of the obstacle and zero flux (zero Neumann boundary condition) at the edge of the whole domain.

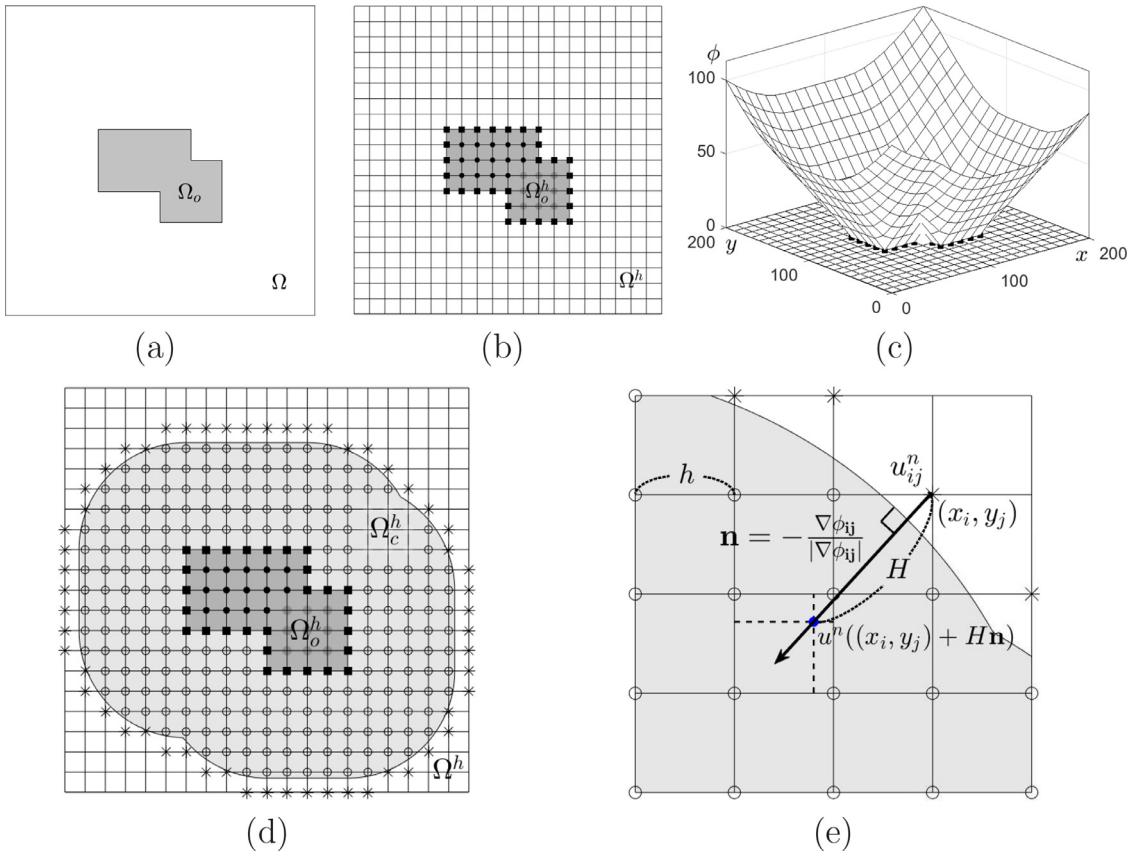

Fig. 1. Schematic of (a) whole domain embedding the given obstacle region, (b) discretization of the whole domain which has the obstacle region, (c) mesh plot of distance function from the given obstacle region, (d) computational domain, and (e) normal vector from the ghost point.

4. Numerical experiments

In this section, we demonstrate the robustness and accuracy of the proposed method through several numerical experiments. The authors in Sherratt et al. [1] showed that the generation of regular and irregular periodic waves by obstacles according to model parameters. First, we perform the same experiments presented in Sherratt et al. [1]. We use the spatial step size $h = 0.5$ and temporal step size $\Delta t = 0.01$ on the domain $\Omega = (0, 400) \times (0, 400)$. We take a square obstacle with an edge length of 20 and is located in the center of the computational domain Ω. The parameter values $A = 1.8,\ B = 1.2,$ and $\delta = 2$ are used. In this paper, unless otherwise stated, the initial condition is given as

$$u(x, y, 0) = \text{rand}(x, y) \text{ and } v(x, y, 0) = \text{rand}(x, y) \text{ for } (x, y) \in \Omega_c^h, \quad (9)$$

where rand(x, y) is a uniform random number between 0 and 1. Fig. 2(a) and (b) show the distributions of prey (v) and predator (u), respectively, at time $t = 1000$ with $C = 4.9$. Fig. 2(c) and (d) show the distributions of prey (v) and predator (u), respectively, at time $t = 1000$ with $C = 6$. We obtain the qualitatively similar results, i.e., regular and irregular patterns, to those previously reported in Sherratt et al. [1].

4.1. Effect of domain

In this section, we check the domain size effect for the same obstacle. We use the spatial step size $h = 0.5$ and temporal step size $\Delta t = 0.01$ on the domain $\Omega = (0, 400) \times (0, 400)$, $(0, 800) \times (0, 800)$, and $(0, 1600) \times (0, 1600)$. We take a square obstacle with an edge length of 20. The parameter values used are $A = 1.8,\ B = 1.2,\ \delta = 2,\ C = 6$. Fig. 3(a)–(c) show the numerical results on the computational domain $\Omega = (0, 400) \times (0, 400)$, $(0, 800) \times (0, 800)$, and $(0, 1600) \times (0, 1600)$, respectively. From top to bottom, each row is the simulation results at $t = 300,\ 800,$

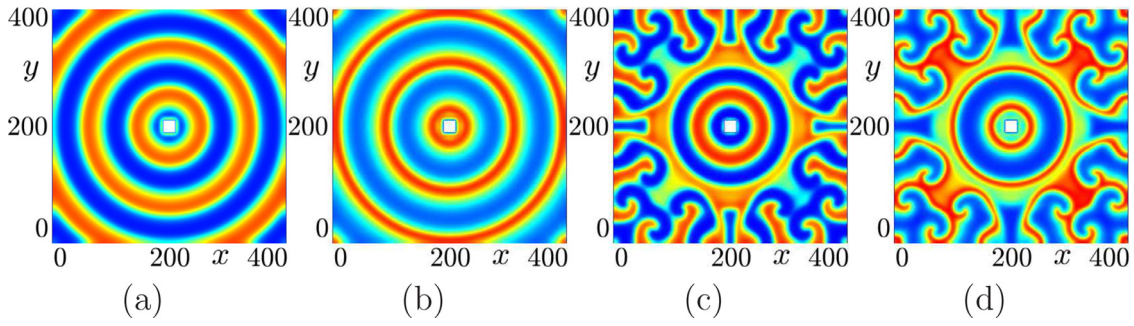

Fig. 2. Travelling wave solutions with an obstacle at time $t = 1000$: (a) and (b) are distributions of prey (v) and predator (u), respectively, with $C = 4.9$; (c) and (d) are distributions of prey (v) and predator (u), respectively, with $C = 6$. Here, $A = 1.8,\ B = 1.2,$ and $\delta = 2$ are used.

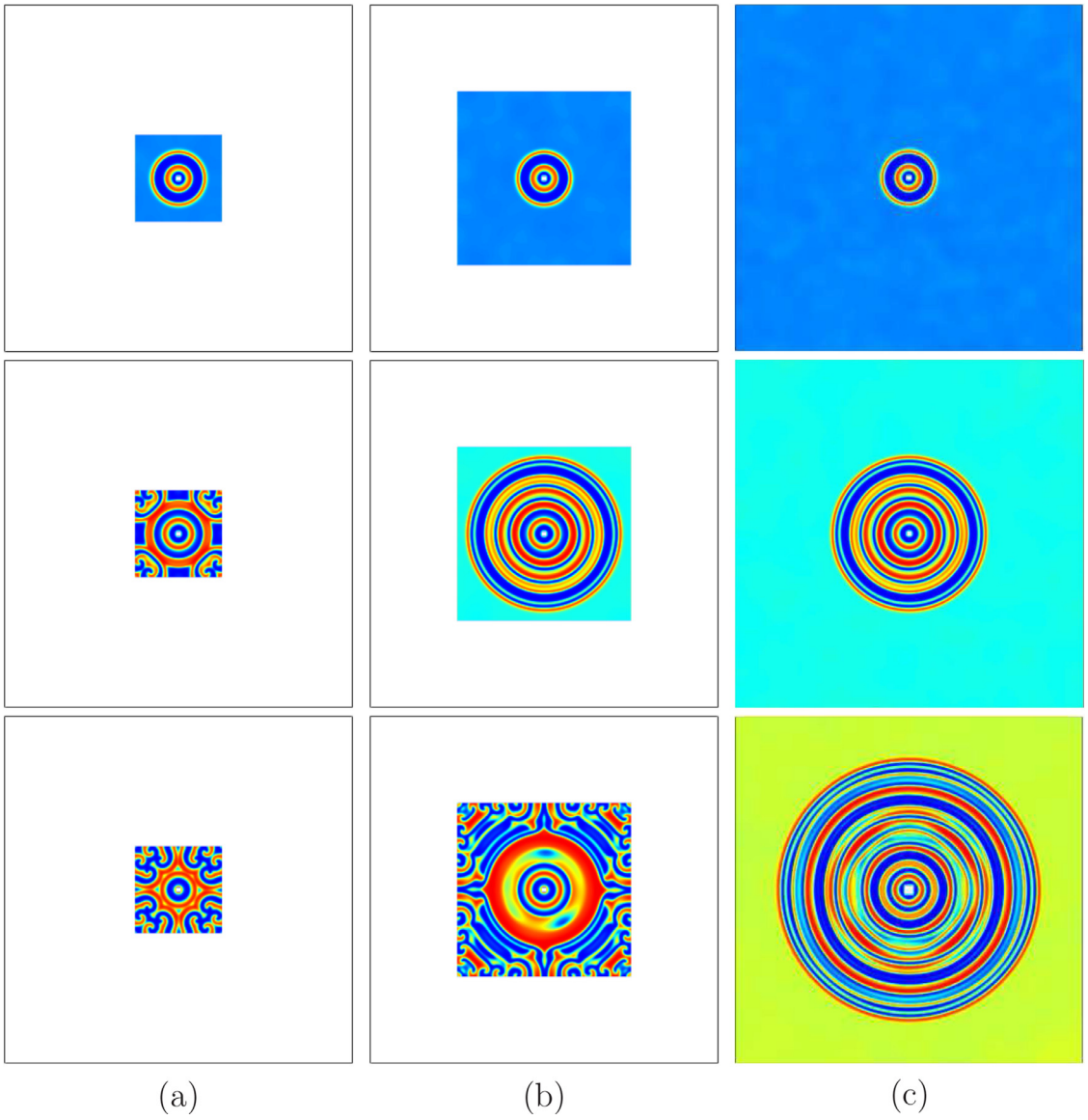

Fig. 3. Temporal evolution of reaction-diffusion system. From top to bottom, each row is the simulation results at $t = 300,\ 800,$ and 1300, respectively. (a), (b), and (c) are the results on the computational domain $\Omega = (0, 400) \times (0, 400)$, $(0, 800) \times (0, 800)$, and $(0, 1600) \times (0, 1600)$, respectively.

and 1300, respectively. We can observe that the chaotic pattern only occurs on the smallest domain $\Omega = (0, 400) \times (0, 400)$ at $t = 800$. Furthermore, at later time $t = 1300$, the chaotic pattern is observed in both the domains $\Omega = (0, 400) \times (0, 400)$ and $\Omega = (0, 800) \times (0, 800)$. These results suggest that the chaotic pattern can be generated from the numerical treatment of the exterior boundary condition.

4.2. Numerical experiments with the proposed method

In this section, we perform several numerical experiments to demonstrate the proposed method can produce a regular periodic wave pattern on a relatively small computational domain. Unless otherwise stated, we use the spatial step size $h = 0.5$ on the domain $\Omega = (0, 400) \times (0, 400)$, temporal step size $\Delta t = 0.01$, and model parameters $A = 1.8,\ B = 1.2,\ \delta = 2,\ C = 6$.

The first example is the square obstacle with an edge length of 20. Fig. 4(a)–(c) show the temporal evolution of the solutions of prey (v) at $t = 300,\ 900,$ and 1500, respectively. We can clearly observe the periodic travelling wave solutions for a reaction-diffusion system on the square fitted domain.

The regular and irregular periodic waves are generated by an obstacle according to model parameters. The proposed method is designed to avoid unwanted chaotic behavior caused by domain boundary effects. Therefore, there are a set of parameters that generate irregular patterns according to model parameters. Fig. 5(a)–(c) show the temporal evolution of the solutions of prey (v) at $t = 300,\ 900,$ and 1500, respectively. Here, $A = 3.1,\ B = 1.2,\ \delta = 2,$ and $C = 6$ are used. We can observe the chaotic wave solutions for a reaction-diffusion system on the square fitted domain.

The second example is the large scale landscape obstacles such as the Kielder Water in northern Britain and the Lake Inari in Fennoscandia. This computational experiment demonstrates that the proposed numerical method produces the regular periodic dynamics for a reaction-diffusion system with complex geometric landscapes. The Kielder Forest is located on the border between England and Scotland and surrounds the Kielder Water. The Kielder Forest is a representative example of a study of periodic waves in a population. Spatio-temporal patterns, similar to periodic travelling waves, were observed in natural populations such as field vole living in the Kielder Forest [20]. The pattern moves in a line about 72° from the north and its direction is almost orthogonal

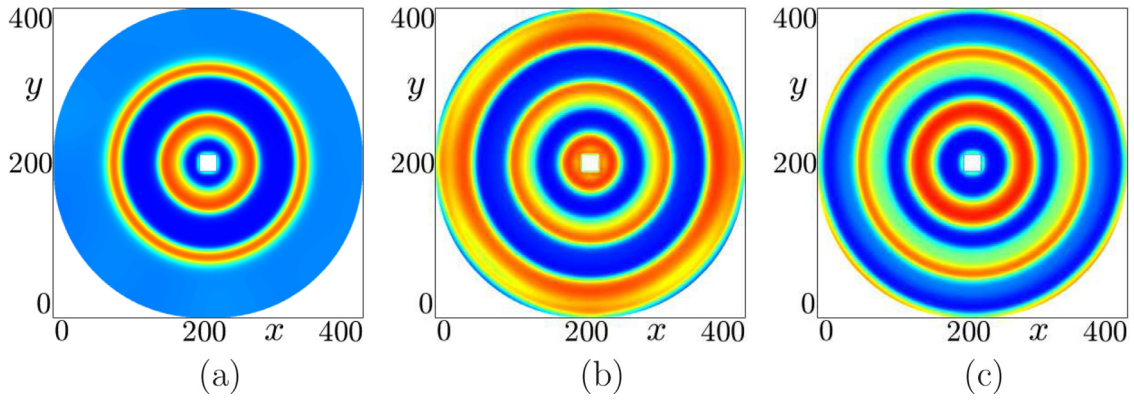

Fig. 4. Temporal evolution of reaction-diffusion system with a square obstacle. (a), (b), and (c) are the solutions of prey (v) at $t = 300$, 900, and 1500, respectively.

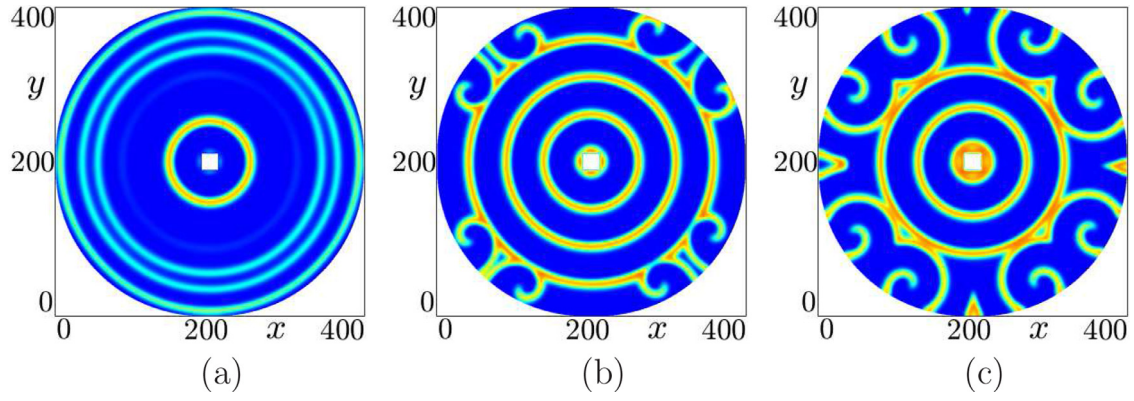

Fig. 5. Temporal evolution of reaction-diffusion system with a square obstacle. (a), (b), and (c) are the solutions of prey (v) at $t = 300$, 900, and 1500, respectively. Here, $A = 3.1$, $B = 1.2$, $C = 6$, and $\delta = 2$ are used.

to the Kielder Water. Meanwhile, the lake Inari is located on the Northern part of Lapland and surrounded by forests mostly composed of pine. The lake Inari has received attention for the cycle in the population of microtine rodents. The population of rodents in Lake Inari was observed like periodic travelling waves [16]. Therefore, the above two examples can be thought of as obstacles in an environment in which natural periodic waves are observed. Assuming that these patterns were caused by predator-prey relationships, studies for periodic travelling waves were conducted based on the predator-prey models [5,21]. The first and second rows in Fig. 6 are the experimental results for the Kielder Water and the Lake Inari, respectively. Fig. 6(a)–(c) show the temporal evolution of the solutions of prey (v) at $t = 300$, 800, and 1300, respectively. We can clearly observe the periodic travelling wave solutions for a reaction-diffusion system on the complicated geometric landscape fitted domain.

The third example is the travelling wave solution for three obstacles of different shapes. The obstacles are triangle, square, and disk of different sizes. Depending on the size of the obstacle, different waves are generated, and the periodic travelling wave solution with three obstacles is dominated by waves generated by the largest obstacle. Fig. 7(a)–(c) show the temporal evolution of the solutions of prey (v) at $t = 300$, 800, and 1300, respectively. We can clearly observe that the periodic travelling wave solutions for a reaction-diffusion system on the fitted domain for the obstacles of various shapes.

Finally, we consider the spatially varying parameters in reaction-diffusion system. We used diffusion coefficient $\delta(x, y) = 0.2$ on $0 \le y < 200$ and $\delta(x, y) = 2$ on $200 \le y \le 400$ to consider spatial inhomogeneity, as illustrated in Fig. 8 (a). Fig. 8(b) shows the snapshot of the solutions of prey (v) at $t = 1300$. We can clearly observe the different solution patterns for a reaction-diffusion system on the fitted domain for the obstacles with inhomogeneity.

We have used the FDM to solve the reaction-diffusion equations. Furthermore, we can also use the FEM and perform the same numerical tests. Fig. 9 shows the solutions that are patterns of prey (v) using Freefem++ which is the free software package to solve partial differential equations in FEM. We can clearly observe that the periodic travelling wave solutions for a reaction-diffusion system on the fitted domain for the obstacles of various shapes using FEM.

4.3. Comparison circular domain with the proposed method

In this section, we perform numerical experiments to compare the solution pattern of the reaction-diffusion system on landscape fitted domain and on the simple domain as a circular exterior boundary. We use the spatial step size $h = 0.5$ on the domain $\Omega = (0, 400) \times (0, 400)$, temporal step size $\Delta t = 0.01$, and model parameters $A = 1.8$, $B = 1.2$, $\delta = 2$, $C = 6$.

The first example is the square obstacle with an edge length of 20. Fig. 10(a) and (b) show the snapshots of the solutions of prey (v) at $t = 1500$ on the circular domain and the landscape fitted domain, respectively. We can clearly observe the periodic travelling wave solutions for a reaction-diffusion system on the two domains.

The second example is the triangle obstacle. Fig. 11(a) and (b) show the snapshots of the solutions of prey (v) at $t = 1400$ on the circular domain and the landscape fitted domain, respectively. A regular wave pattern is generated with the square obstacle on the circular domain in Fig. 10(a) while an irregular wave pattern is generated with the triangular obstacle on the circular domain

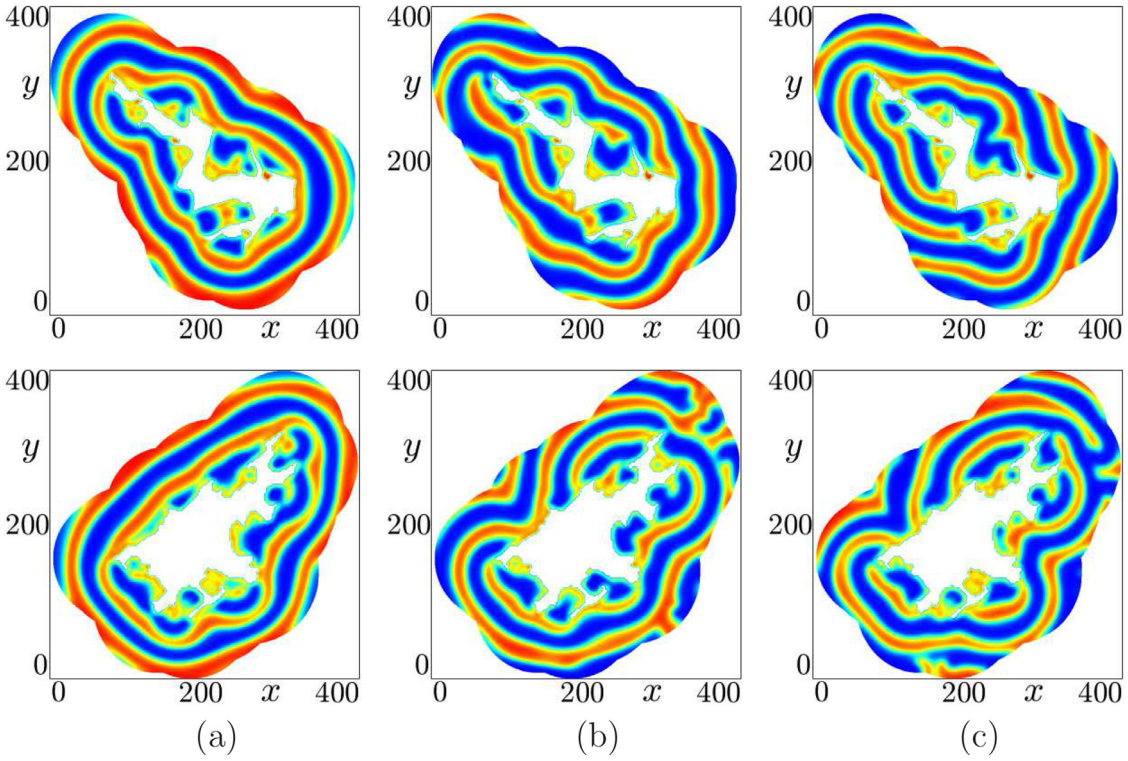

Fig. 6. Temporal evolutions of reaction-diffusion system with the Kielder Water in northern Britain (top row) and the Lake Inari in Fennoscandia (bottom row). (a), (b), and (c) are the solutions of prey (v) at $t = 300$, 800, and 1300, respectively.

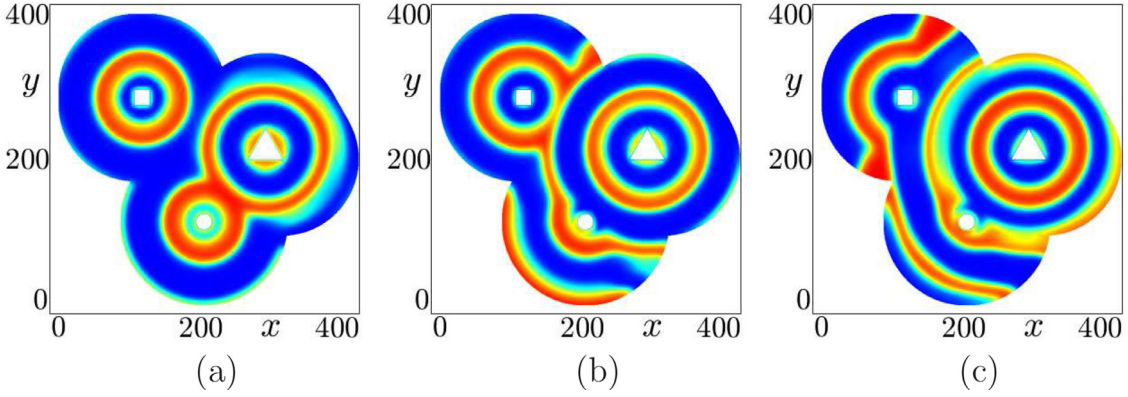

Fig. 7. Temporal evolutions of reaction-diffusion system with three obstacles of different shapes. (a), (b), and (c) are the solutions of prey (v) at $t = 300$, 800, and 1300, respectively.

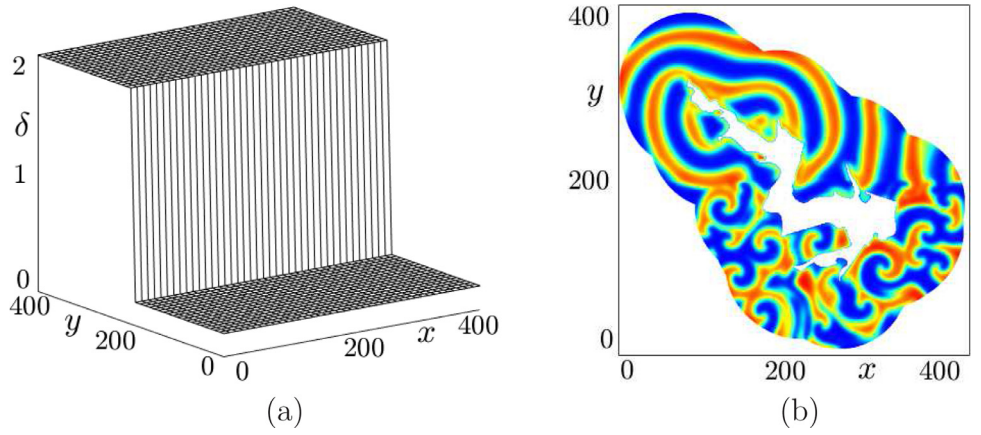

Fig. 8. (a) Illustration of spatially varying diffusion coefficient δ and (b) snapshot of the numerical solutions of prey (v) with inhomogeneous diffusion coefficient on the fitted domain for the Kielder water at $t = 1300$.

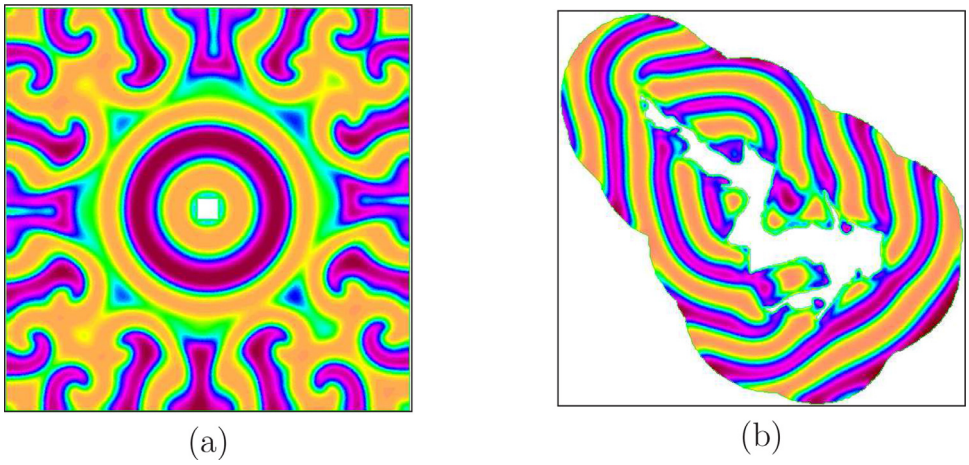

Fig. 9. Using Freefem++, snapshots of the solutions with obstacles, a square and the Kielder Water.

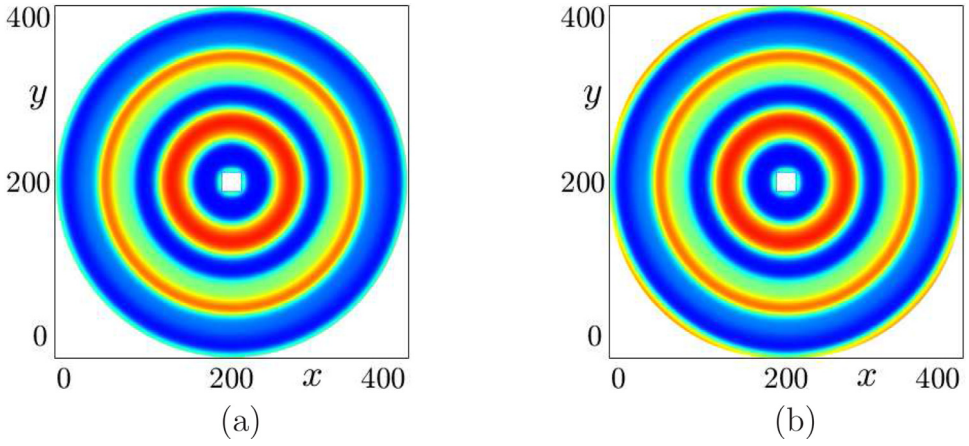

Fig. 10. Snapshots of the solutions of prey (v) with the square obstacle at $t = 1500$ on (a) the circular domain and (b) the landscape fitted domain.

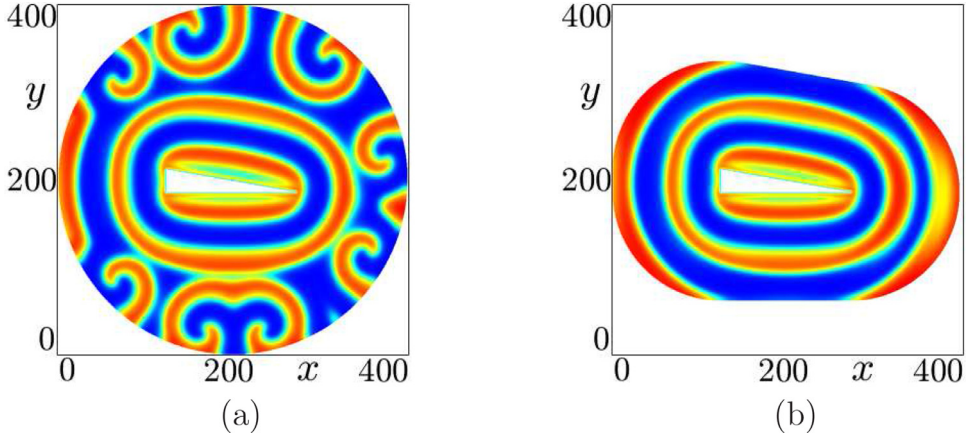

Fig. 11. Snapshots of the solutions of prey (v) with the triangle obstacle at $t = 1400$ on (a) the circular domain and (b) the landscape fitted domain.

in Fig. 11(a). However, we can observe the regular periodic travelling wave solutions for a reaction-diffusion system on the proposed method, i.e., on the landscape fitted domain in Figs. 10(b) and 11(b). If the pattern shape formed by the obstacle is similar to a circle, the patterns on the circular domain and landscape fitted domain are generated a regular wave pattern, but if not, an irregular wave pattern is generated on the circular domain. The proposed method generated the periodic travelling wave pattern on the arbitrary obstacle with model parameter $A = 1.8, B = 1.2, \delta = 2, C = 6$.

4.4. Vegetation model

In this section, we consider the Klausmeier model [17] on a domain Ω:

$$\frac{\partial w}{\partial t}(\mathbf{x}, t) = A - Lw(\mathbf{x}, t) - Rw(\mathbf{x}, t)u^2(\mathbf{x}, t) + V\frac{\partial w}{\partial x}(\mathbf{x}, t), \tag{10}$$

$$\frac{\partial u}{\partial t}(\mathbf{x}, t) = RJw(\mathbf{x}, t)u^2(\mathbf{x}, t) - Mu(\mathbf{x}, t) + D\Delta u(\mathbf{x}, t), \tag{11}$$

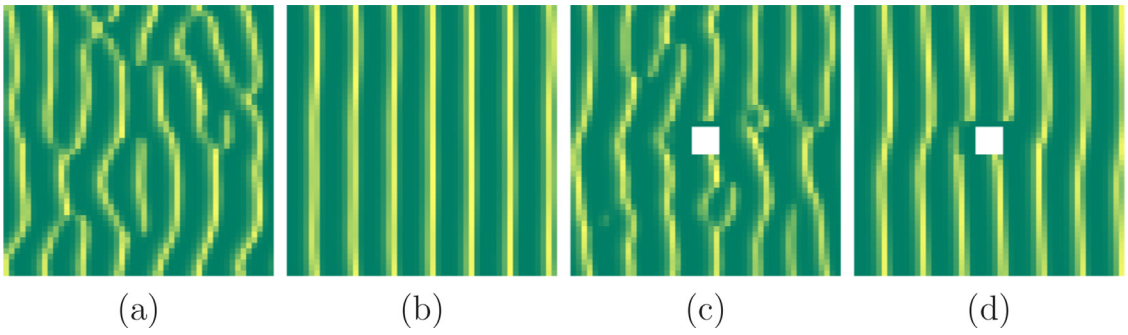

Fig. 12. Vegetation patterns on the landscape with and without an obstacle: (a) and (b) are distributions of vegetation biomass (u) without an obstacle at $t = 100$ and $t = 1000$, respectively; (c) and (d) are distributions of vegetation biomass (u) with an obstacle at $t = 100$ and $t = 1000$, respectively. Here, $\Delta t = 1$, $h = 4$, $A = 2$, $M = 0.45$, $V_0 = 182.5$ and $N_x = N_y = 50$ are used.

where $\mathbf{x} = (x, y) \in \Omega \subset \mathbb{R}^2$, $t > 0$, and w and u are water resource and vegetation biomass, respectively. Let us define the non-dimensional parameters as $w^* = R^{1/2}L^{-1/2}Jw$, $u^* = R^{1/2}L^{-1/2}u$, $t^* = Lt$, $\mathbf{x}^* = L^{1/2}D^{-1/2}\mathbf{x}$, $A^* = AR^{1/2}L^{-3/2}J$, $M^* = ML^{-1}$, $V_0^* = VL^{-1/2}D^{-1/2}$. Then, Eqs. (10) and (11) become the following non-dimensional equations after dropping the asterisks:

$$\frac{\partial w}{\partial t}(\mathbf{x}, t) = A - w(\mathbf{x}, t) - w(\mathbf{x}, t)u^2(\mathbf{x}, t) + V_0\frac{\partial w}{\partial x}(\mathbf{x}, t),$$
$$\frac{\partial u}{\partial t}(\mathbf{x}, t) = w(\mathbf{x}, t)u^2(\mathbf{x}, t) - Mu(\mathbf{x}, t) + \Delta u(\mathbf{x}, t).$$

The authors in Zhang et al. [22] showed that the generation of regular and irregular vegetation patterns in semiarid regions. We perform the same experiments presented in Zhang et al. [22] on a domain embedding an obstacle region. We solve the following discrete Eqs. (12) and (13) on Ω_c^h:

$$\frac{w_{ij}^{n+1} - w_{ij}^n}{\Delta t} = A - w_{ij}^n - w_{ij}^n(u_{ij}^n)^2 + V_0(w_x^n)_{ij}, \tag{12}$$

$$\frac{u_{ij}^{n+1} - v_{ij}^n}{\Delta t} = w_{ij}^n(u_{ij}^n)^2 - Mu_{ij}^n + \Delta_d u_{ij}^n. \tag{13}$$

Let us discretize the rectangular domain $\Omega = (L_x, R_x) \times (L_y, R_y)$ using a uniform spatial step size $h = (R_x - L_x)/N_x = (R_y - L_y)/N_y$, where N_x and N_y are positive integers. Let $\Omega^h = \{(x_i, y_j) | x_i = L_x + (i-1)h,\ 1 \le i \le N_x$ and $y_j = L_y + (j-1)h,\ 1 \le j \le N_y\}$ be a discrete domain, Ω_o^h be the discrete obstacle domain and computational domain $\Omega_c^h = \Omega^h \backslash \Omega_o^h$. The numerical solutions to $w(x, y, t)$ and $u(x, y, t)$ are approximated at cell-corners by $w_{ij}^n \equiv w(x_i, y_j, n\Delta t)$ and $u_{ij}^n \equiv u(x_i, y_j, n\Delta t)$, where Δt is the temporal step size. The Dirichlet boundary condition and the periodic boundary condition are applied on the obstacle boundary and the exterior boundary, respectively. To validate for solving the solution pattern of vegetation model, we use same model parameter values in Zhang et al. [22]. Fig. 12(a) and (b) show the biomass density (u) at time $t = 100$ and $t = 1000$, respectively. Fig. 12(c) and (d) show the biomass density (u) on the landscape with the square obstacle at time $t = 100$ and $t = 1000$, respectively. We obtain the qualitatively similar results, i.e., striped vegetation patterns, to those previously reported in Zhang et al. [22].

5. Conclusion

In this paper, we presented a novel landscape fitted domain construction and its boundary treatment of periodic travelling wave solutions for a diffusive predator-prey system with landscape features. In the case of periodic travelling wave solutions, the boundary treatment is critical because it may result in unexpected chaotic pattern. To avoid this unwanted chaotic behavior, we need to use sufficiently large computational domain to minimize the boundary treatment effect. However, a large domain has high computational costs for getting a solution. Hence, in the proposed method, we defined the landscape fitted domain using the distance function based on the obstacle. Using the level set function and interpolations, the values at the ghost points were interpolated in the normal direction of the exterior boundary. At the interior boundary, we used homogeneous Dirichlet boundary condition. We can observe that a regular periodic wave pattern on a relatively small computational domain by applying the proposed method through several numerical experiments. We demonstrated the robustness and accuracy of the proposed method through the real complicated landscape such as the Kielder Water and the Lake Inari.

Declaration of Competing Interest

The authors declare that they have no known competing financial interests or personal relationships that could have appeared to influence the work reported in this paper.

CRediT authorship contribution statement

Sangkwon Kim: Writing - original draft, Methodology, Conceptualization, Software, Writing - review & editing. **Jintae Park:** Writing - original draft, Software, Validation, Visualization, Writing - review & editing. **Chaeyoung Lee:** Visualization, Investigation, Validation, Writing - review & editing. **Darae Jeong:** Methodology, Investigation, Supervision. **Yongho Choi:** Investigation, Validation. **Soobin Kwak:** Visualization, Writing - review & editing. **Junseok Kim:** Conceptualization, Methodology, Project administration, Funding acquisition.

Acknowledgments

The corresponding author (J. Kim) was supported by Basic Science Research Program through the National Research Foundation of Korea (NRF) funded by the Ministry of Education (NRF-2019R1A2C1003053). The authors greatly appreciate the reviewers for their constructive comments and suggestions, which have improved the quality of this paper.

References

[1] Sherratt JA, Lambin X, Thomas CJ, Sherratt TN. Generation of periodic waves by landscape features in cyclic predator-prey systems. Proc R Soc Lond B 2002;269:327–34.
[2] Sherratt JA, Lambin X, Sherratt TN. The effects of the size and shape of landscape features on the formation of traveling waves in cyclic populations. Am Nat 2003;162:503–13.
[3] Babloyantz A, Sepulchre JA. Target and spiral waves in oscillatory media in the presence of obstacles. Phys D 1991;49(1–2):52–60.

[4] Smith MJ, Sherratt JA, Armstrong NJ. The effects of obstacle size on periodic travelling waves in oscillatory reaction-diffusion equations. Proc Math Phys Eng Sci 2008;464:365–90.
[5] Yun A, Shin J, Li Y, Lee S, Kim J. Numerical study of periodic traveling wave solutions for the predator-prey model with landscape features. Int J Bifurc Chaos 2015;25(9):1550117.
[6] Garvie MR, Burkardt J, Morgan J. Simple finite element methods for approximating predator-prey dynamics in two dimensions using Matlab. Bull Math Biol 2015;77(3):548–78.
[7] Liu Q, Jiang D. Stationary distribution and extinction of a stochastic predator-prey model with distributed delay. Appl Math Lett 2018;78:79–87.
[8] Alharbi W, Petrovskii S. Patterns of invasive species spread in a landscape with a complex geometry. Ecol Complex 2018;33:93–105.
[9] Yue X, Wang F, Hua Q, Qiu XY. A novel space-time meshless method for non-homogeneous convection-diffusion equations with variable coefficients. Appl Math Lett 2019;92:144–50.
[10] Sherratt JA. Numerical continuation methods for studying periodic travelling wave (wavetrain) solutions of partial differential equations. Appl Math Comput 2018;218(9):4684–94.
[11] Gani MO, Ogawa T. Stability of periodic traveling waves in the Aliev–Panfilov reaction-diffusion system. Commun Nonlinear Sci 2016;33:30–42.
[12] Gani MO, Ogawa T. Spiral breakup in a RD system of cardiac excitation due to front-back interaction. Wave Motion 2018;79:73–83.
[13] Tlidi M, Clerc MG, Escaff D, Couteron P, Messaoudi M, Khaffou M, Makhoute A. Observation and modelling of vegetation spirals and arcs in isotropic environmental conditions: dissipative structures in arid landscapes. Philos Trans R Soc A 2018;376(2135):20180026.
[14] Bordeu I, Clerc MG, Couteron P, Lefever R, Tlidi M. Self-replication of localized vegetation patches in scarce environments. Sci Rep 2016;6:33703.
[15] Smith NJ, Glaser R, Hui VW, Lindner JF, Manz N. Disruption and recovery of reaction-diffusion wavefronts colliding with obstacles. Phys A 2019;517:307–20.
[16] Heikkilä J, Below A, Hanski I. Synchronous dynamics of microtine rodent populations on islands in Lake Inari in northern fennoscandia: evidence for regulation by mustelid predators. Oikos 1994;70:245–52.
[17] Klausmeier CA. Regular and irregular patterns in semiarid vegetation. Science 1999;284(5421):1826–8.
[18] Duan D, Niu B, Wei J. Hopf-Hhopf bifurcation and chaotic attractors in a delayed diffusive predator-prey model with fear effect. Chaos Soliton Fractals 2019;123:206–16.
[19] Kumar S, Kharbanda H. Chaotic behavior of predator-prey model with group defense and non-linear harvesting in prey. Chaos Soliton Fractals 2019;119:19–28.
[20] Sherratt TN, Lambin X, Petty SJ, Mackinnon JL, Coles CF, Thomas CJ. Use of coupled oscillator models to understand synchrony and travelling waves in populations of the field vole Microtus agrestis in northern England. J Appl Ecol 2000;37:148–58.
[21] Sherratt JA, Smith MJ. Periodic travelling waves in cyclic populations: field studies and reaction-diffusion models. J R Soc Interface 2008;5(22):483–505.
[22] Zhang H, Huang T, Dai L, Pan G, Liu Z, Gao Z, et al. Regular and irregular vegetation pattern formation in semiarid regions: a study on discrete Klausmeier model. Complexity 2020.